



A consecutive methanation scheme for conversion of CO₂ – A study on Ni₃Fe catalyst in a short-contact time micro packed bed reactor

Sarvenaz Farsi, Wolfgang Olbrich, Peter Pfeifer*, Roland Dittmeyer

Institute for Micro Process Engineering at Karlsruhe Institute of Technology, Hermann-von-Helmholtz-Platz 1, 76344 Eggenstein-Leopoldshafen, Germany

ARTICLE INFO

Keywords

Kinetic rate modeling
Microstructured reactor
Carbon dioxide methanation
Carbon monoxide
Reverse-water gas shift reaction

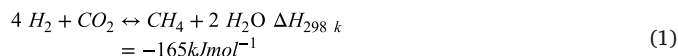
ABSTRACT

In this work, the kinetics of CO₂ methanation reaction is investigated on a 17 wt% Ni₃Fe/γ-Al₂O₃ catalyst under technical operation conditions of Power-to-Gas processes. A short-contact time microstructured packed bed reactor with internal cross-flow cooling channel was designed particularly for kinetic studies of the highly exothermic methanation reaction. The influence of temperature, pressure, reactant and product composition as well as residence time on the product composition and conversion of the reactants was carefully studied. In total more than 160 data points were collected and fitted to three literature models applying a non-isothermal reactor model. Based on the state-of-the-art kinetic models and the experimental observations, a new LHHW rate equation for the consecutive CO₂ methanation reaction was developed. This new model has reasonably lower number of parameters and improves description of the reaction compared to literature models with regard to the Ni₃Fe catalyst system. Special attention was paid to the selectivity behavior and the influence of carbon monoxide and water on the reaction.

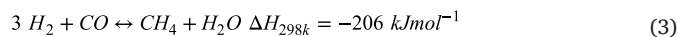
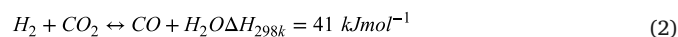
1. Introduction

A major hurdle in application of renewable energy is the strong fluctuation of wind and sun. So far, these fluctuations have been mainly compensated with conventional power plants, which contribute to CO₂ emission. In order to tackle the production and consumption mismatch over day-and season-scale, one very promising concept for storage of large amounts of energy is the so-called Power-to-X (PtX) technology, where regional and time-dependent surplus energy from renewable sources is converted into value-added compounds. The technologies which aim for hydrogen or methane as products are summarized under Power-to-Gas (PtG) processes. Transportation and storage of large quantities of hydrogen requires new infrastructure whereas the infrastructure for transportation and storage of methane already exists. Moreover, in terms of energy per volume methane has advantages over hydrogen, which are important at least for applications in mobility [1,2]. Additionally, as a result of the Paris agreement in December 2015, the share of CO₂ emissions must be reduced drastically, imposing new strategies to reduce the number of power plants and enhance technologies which contribute to CO₂ reduction [3]. Conversion of renewable H₂ alongside with biogenic CO₂ or CO₂ from air into methane is considered one of the most promising technologies in the latter context.

The catalytic hydrogenation of CO₂ was discovered by Paul Sabatier in 1902 [4] is technically relevant in different fields, such as gas purification for synthesis gas, and adjustment of H₂/C ratio in biomass or coal gasification processes [5–7]. The reaction of hydrogen and carbon dioxide to methane is a highly exothermic reaction, limited by thermodynamic equilibrium and is accompanied with volume reduction, as given in Equation (1):



The catalytic CO₂ methanation is typically assumed to be a two-step reaction with reverse water gas shift (rWGS, Equation (2)) as the first step, followed by CO methanation (Equation (3)). However, the true mechanism of the reaction is still under debate.



Since Sabatier's discovery, many groups have studied methanation reaction of CO₂ or CO with diverse motivation, applying different catalysts and experimental conditions. Early publications on methanation kinetics were done in the 1950s [8,9]. Further developments on the models for application in gas purification and methane-steam-reform-

* Corresponding author.

E-mail address: peter.pfeifer@kit.edu (P. Pfeifer)

ing were mainly carried out in the 1980s [10–12]. The kinetic model published by Xu and Froment [11], which studied the methane steam reforming reaction on an aged Ni/MgAl₂O₄ catalyst, can be understood as pioneering work for further work on methanation kinetics. In their work, a set of reaction rate coefficients for the reversible reactions (CO and CO₂ methanation and rWGS reaction) are suggested. A summary of accompanied and following studies can be found elsewhere [13,14]. Despite a considerable number of developed rate equations and studies delivering rate constants for the methanation of CO and/or CO₂, only a few of the studies deliver data under relevant operating conditions [13]. For example, most of the studies are carried out under very low reaction temperature and pressures [12,15–17]. Whereas, the typical operation regime in technical plants is a temperature window of 300–450 °C and a pressure of 5–20 bar [14].

The model developed by Koschany et al. [18] was developed for power to gas applications on Ni catalysts with pure CO₂ in the feed. The process parameters are varied between 180 and 340 °C, 1–15 bar and H₂:CO₂ ratio of 0.25 to 8. Prior to the kinetic data collection, the catalyst was aged for 300 h to reach a constant level of activity during kinetic measurements. Koschany et al. could show that a power law rate equation can be applied to describe the experimental data fairly good; however, it fails to describe the conversions close to thermodynamic equilibrium. The authors solved this problem by developing a model with inhibition term upon Langmuir-Hinshelwood-Hougen-Watson (LHHW) formalism. The model fails to describe methane selectivity, and can be only used for description of CO₂ conversion, since it completely ignores CO formation.

Kopyschinski [19] studied the CO methanation together with WGS reaction. He applied a spatially resolved wall-coated plate reactor for data collection using a commercial nickel catalyst. The reaction conditions applied were a temperature window of 280–360 °C, pressure of 1 bar and H₂:CO₂ ratio of 5–6. According to Kopyschinski, CH₄ and CO₂ do not inhibit the reaction rate, in contrast to water, which clearly contributes to the rate inhibition. Unfortunately, no equilibrium term was included in these models, which makes them useless for description of technical reactors

Zhang et al. [20] investigated the methanation reaction using biomass-based synthesis gas and used mixtures of CO and CO₂ in the feed. The temperature and pressure were varied from 275 to 360 °C and 1 to 5 bar. The kinetic rate models used were adapted from the work of Xu and Froment [11] and fitted to the collected data. Essential insights achieved by Zhang et al. are that CO₂ has no influence on the rate of CO methanation and that higher H₂:CO ratio improves the methane selectivity significantly. All other species taking part in the reaction (CH₄, CO, H₂ and H₂O) are included in the inhibition term. In Table 1 the mathematical description of the Koschany, Kopyschinski and the Zhang models are presented according to the equation (4). The equations are

Table 1
Overview of LHHW kinetic rate models in literature for industrial operational conditions.

Model	reaction	(Rate constant) × (driving force)	inhibition term (reciprocal of adsorption term)	equilibrium term
Koschany [18]	$r_{(CO_2 \rightarrow CH_4)}$	$k \cdot p_{CO_2}^{0.5} p_{H_2}^{0.5}$	$\frac{1}{(1 + K_{OH} \frac{p_{H_2O}}{p_{H_2}} + K_{H_2} p_{H_2}^{0.5} + K_{CO_2} p_{CO_2}^{0.5})^2}$	$1 - \frac{p_{CH_4} p_{H_2}^2 p_{H_2O}^2}{p_{CO_2} p_{H_2}^2 K_{eq}}$
Kopyschinski [19]	$r_{(CO_2 \rightarrow CO)}$	$k_1 \cdot p_{CO_2} p_{H_2}^{0.5}$	$\frac{1}{(1 + K_C p_{CO} + K_{OH} \frac{p_{H_2O}}{p_{H_2}})^2}$	$1 - \frac{p_{CO} p_{H_2O}}{p_{CO_2} p_{H_2} K_{WGS}}$
Zhang [20]	$r_{(CO \rightarrow CH_4)}$	$k_2 \cdot p_{CO}^{0.5} p_{H_2}^{0.5}$	$\frac{1}{(1 + K_{CO} p_{CO} + K_{H_2} p_{H_2} + K_{CH_4} p_{CH_4} + K_{H_2O} \frac{p_{H_2O}}{p_{H_2}})^2}$	–
	$r_{(CO_2 \rightarrow CO)}$	$k \cdot p_{CO_2}$		$1 - \frac{p_{CO} p_{H_2O}}{p_{CO_2} p_{H_2} K_{WGS}}$
	$r_{(CO \rightarrow CH_4)}$	$k \cdot p_{CO} p_{H_2}^{0.5}$		$1 - \frac{p_{CH_4} p_{H_2}^2 p_{H_2O}^2}{p_{CO_2} p_{H_2}^2 K_{CO-Meth.}}$

adapted to the further notation in this work.

$$r = \frac{(\text{rate constant}) \times (\text{driving force}) \times (\text{equilibrium term})}{\text{adsorption term}} \quad (4)$$

In general, most of the literature works addressed Al₂O₃ supported Ni catalysts or Ni supported on other compounds, e.g. TiO₂, SiO₂ etc. [13]. Due to the ubiquitous deactivation of the Nickel catalysts, most of the authors were obliged to run a pretreatment of the catalyst in order to reach a stable catalyst activity before collecting kinetic data [11,18] or change the catalyst every few hours [20]. Mutz et al. studies proved the superior activity of a 17 wt% Ni₃Fe catalyst supported on γ-Al₂O₃ compared to a mono metallic Ni catalyst. In addition, experimental tests in a microstructured packed bed reactor for a duration of 45 h showed higher methane selectivity and stability of the Ni₃Fe compared to a commercial Ni catalyst [21]. Serrer et al. carried out detailed operando investigations on a monometallic Ni catalyst and a bimetallic Ni₃Fe-γ-Al₂O₃ in cycles of over- and under-stoichiometric conditions of hydrogen. They showed that under H₂-deficient conditions, the monometallic Ni catalyst is more prone to irreversible surface oxidation. Whereas in case of applying Ni-Fe catalyst, a preferential and reversible FeO is formed which protects the active Ni sites from oxidation. In this respect, iron is confirmed to play a protective role and preserves the catalytic activity under PtG operational conditions [22].

As the monometallic Ni catalyst stability seems problematic, the present study undertakes a systematic approach for investigating the kinetics of a fresh 17 wt% Ni₃Fe catalyst for the CO₂ methanation reaction in a microstructured packed bed reactor with internal cross flow cooling structure to suggest a data and rate equation set which can be further used for describing a reactor under technical process conditions. The catalyst temperature could be monitored in the microreactor. The kinetics are analyzed with a non-isothermal reactor model, based on experimental observations. The operation parameters are T = 300–450 °C and p = 2–18 bar. They are chosen based on real operating conditions for reactors in PtG methanation plants, that are developed in our working group [23]. The relevant models in literature are compared and fitted to the experimental data collected. A two-step reaction rate model for CO₂ methanation with fewer number of parameters based on Equation (1) and Equation (2) is proposed and its characteristics compared to the literature models applying various statistical methods.

2. Materials and methods

2.1. The microstructured reactor

The kinetic measurements were performed in a microstructured packed bed reactor with internal cross-flow cooling structure as illustrated in Fig. 1, designed and fabricated in our institute. The general reactor concept has been already successfully tested for other applica-

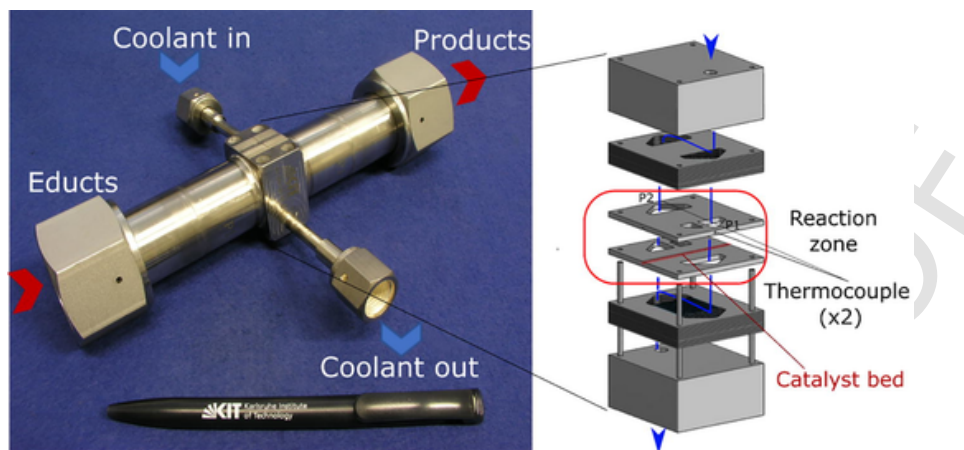


Fig. 1. The microstructured packed bed reactor design used for kinetic measurements.

tions such as methanol, DME and Fischer-Tropsch synthesis [24–26]. Mutz et al. used this general reactor design for CO₂ methanation catalyst performance tests [21], but compared with the present study with much longer packed bed length. Based on the results achieved in these former studies, the reactor applied in this work was optimized for kinetic studies in the exothermic methanation reaction: The enhanced reactor possesses a shorter bed length (20 mm compared to 60 mm in the previous applications) and a different stacking scheme of the microstructured plates to be able to measure the temperature directly adjacent to the reaction zone. In the center of the reactor body, two oppositely structured metal plates form the reaction slit with dimensions of 20 mm (length) × 9 mm (width) × 1.5 mm (depth). On the back side of these plates a slotted hole with a diameter of 1 mm is used for measuring the metal surface temperature 1.5 mm away from the catalyst on the left and right side of the bed at half-length using a K-type thermocouple (marked as P1 and P2). The short bed length allows for operating at short-contact time conditions, without requiring extreme dilution of the catalyst or feed to reach low or intermediate conversion. Also the shorter bed length is beneficial regarding keeping the pressure drop low. The bed temperature or for the sake of preciseness the metal surface temperature near the bed was used for setting the operational boundaries (to avoid formation of hotspots).

Above and under the reaction zone, 16 microstructured metal foils with a thickness of 400 μm are stacked on each other as the cooling structure. Each of these foils contains 19 semicircular channels of 250 μm depth, 500 μm width and 25 mm length, and are arranged perpendicular to the flow direction of the reaction zone. The foil stack is sandwiched between two 16 mm thick metal plates, in which in total four holes are drilled for inserting heating cartridges to heat up the reactor to reaction temperature. The material used for the reactor is an austenitic high temperature-resistant alloy (Nicrofer® 3220) to guaranty the reactor endurance under carburizing, oxidizing and reducing conditions and negligible blank activity, see also elsewhere [23].

2.2. Experimental setup

The experimental setup can be divided into three major parts:

1. Gas supply: In the gas supply part, five SLA5800 series mass flow controllers (MFCs) from Brooks Instruments® and one liquid flow controller (LFC) from Bronkhorst® were integrated. The water dosage was carried out applying a nitrogen pressurized water-tank followed by the LFC and an evaporation pipeline.
2. Reactor: The catalyst was fixed in the reaction bed from both sides by glass wool. All the tubing before the reactor was heated up to reaction temperature. The lines after the reactor were kept at 200 °C

in order to avoid water condensation. Pressure regulation was done using a pressure sensor and an automated Flow-serve® needle valve after the reactor. The pressure drop along the reactor was measured with a pressure difference sensor from DL-Systeme GmbH. Pressurized air was used as the cooling medium to keep the reaction temperature gradient-free in the catalytic bed. The flow rate of the air was adjusted at 40 Nlmin⁻¹ and was always pre-heated to the reaction temperature. For air pre-heating, a micro heat exchanger built at our institute with 15 heating cartridges, 225 W each and electrically heated lines were installed.

3. Analytics: The reaction gases were analyzed by an online Gas chromatograph 7890B from Agilent Technologies. The gas chromatograph was equipped with two columns: HP-Plot/Q 19095P-Q04 and a 5A-Mole sieve 19095P-MS6 and two detectors: a flame ionization detector (FID) and a thermal conductivity detector (TCD). The online data were used for quantification of the CO₂, CO, H₂, H₂O, and N₂ (using TCD) and CH₄ (using FID).

2.3. Experimental conditions and procedure

The kinetic data used for the modeling were collected in the first 50 h of time on stream (TOS), where the activity was proven to be stable. The catalyst was replaced when an activity loss of around 3–5% was measured; therefore the reactor was opened and newly loaded. In total 5 reactor loadings were used for collecting the data and to reproduce data points. After each reactor loading, a reference point ($T = 350$ °C, $H_2/CO_2 = 4$, $p_{abs} = 4$ bar and $\tau_{mod} = 0.38$ mg min mLCO₂⁻¹) was measured which was used for calculation of the standard deviation. Consequently, for all data points the deviation can be calculated using this standard deviation. The kinetic measurements were carried out at nine different temperatures varied between 300 and 450 °C. The pressure ranged from 2 to 18 bar. The modified residence time, which is defined as the mass of the catalyst divided by the volumetric flow rate (at standard temperature and pressure) of CO₂, was varied between 0.09 and 0.72 mg_{cat} min NmLCO₂⁻¹. These parameters were varied under a constant stoichiometric ratio of H₂/CO₂ (=4) and 50% feed dilution with N₂. The flow rate of inert N₂ in the feed was also used as internal standard for calculation of the product flow rate. The tested stoichiometric ratio of H₂ to CO₂ was varied between 2 and 8. In this regard, two sets were examined: in the first set, the p_{H_2} was kept constant at 1.6 bar and p_{CO_2} was changed. In the second set, the p_{CO_2} was kept at 0.4 bar and with p_{H_2} variation different H₂/CO₂ ratios were achieved. In this analysis the modified residence time of CO₂ was kept constant at 0.38 mg_{cat} min NmLCO₂⁻¹ for the sake of comparability. Finally, the influence of water and CO addition in the feed on the product formation/inhibition in relevant concentrations was investigated.

In all the experiments, the catalytic bed was diluted with $\gamma\text{-Al}_2\text{O}_3$ (1/8 in. pellets, Alfa Aesar), crushed to the desired particle fraction, in order to guaranty a homogeneous distribution of the catalyst in the bed and to avoid temperature gradients higher than $+10\text{ }^\circ\text{C}$ between measured temperature inside the foil stack and the setpoint. The mass ratio of catalyst to $\gamma\text{-Al}_2\text{O}_3$ was 2 to 1, when loading the bed with 76 mg catalyst, and 0.7 to 1 at reduced catalyst loading of 47 mg. Both, catalyst and $\gamma\text{-Al}_2\text{O}_3$ were fractioned between 200 and 300 μm to avoid segregation of the particles after being filled in the reactor due to their different physical properties. The synthesis of the catalyst and its detailed characteristics can be found elsewhere [21]. For reduction, the catalyst was heated up to $500\text{ }^\circ\text{C}$ with 5 Kmin^{-1} ramp under a gas flow of 1:1 H_2 and N_2 and total volumetric flow of $900\text{ Nml g}_{\text{cat}}^{-1}\text{ min}^{-1}$. The temperature was kept for two hours at $500\text{ }^\circ\text{C}$. The absolute pressure during the reduction was set to 2.5 bar. Between experiments, the reactor was kept at $300\text{ }^\circ\text{C}$ in reducing atmosphere and flow identical to the reduction procedure to keep the catalyst in reduced state. For each experimental point, the catalyst was operated over 120 min reaction run under a particular condition, and 5 GC measurements were averaged to ensure reproducibility of the data. The reference point was measured every 15 h of reaction run to check for possible catalyst deactivation. Every single data point used for the kinetic modelling was controlled for internal and external mass and heat transport limitation by calculating the Weisz modulus, Carberry number and Mears criterion [27]. The requirements of Carberry and Weisz-Prater are fulfilled. The film and particle overheating criteria for some of the data points exceeded the criteria by a factor of 1.1–1.7, which was considered acceptable for modelling of the reaction kinetics.

2.4. Mathematical methods

2.4.1. The kinetic model

The rate equations developed and tested in this work are formulated based on the Langmuir-Hinshelwood-Hougen-Watson (LHHW) approach. The general form of a LHHW rate equation is given in [28].

In the present work, several prerequisites were desired for final kinetic model:

- The formation of methane from CO_2 occurs through two consecutive reactions with the formation of CO as an intermediate product: the first reaction is the so-called rWGS reaction (Eq. (2)) followed by CO methanation (Eq. (3)). Therefore, the model should be capable of describing the CO yield and selectivity to methane formation.
- The thermodynamic equilibrium of all the reactions should be considered in the model.
- The effective order of the reaction for both reactions must be greater than zero.
- The inhibition of the reaction rate by H_2 , CO, CH_4 and H_2O should be verified by means of the modelling and/or experiments.

2.4.2. Reactor model: non-isothermal PFR

For calculation of the product flows, the catalytic reactor bed was modelled as a non-isothermal, pseudo-homogeneous plug flow reactor (PFR). The mathematical description of the reaction was defined on a steady-state balance, with no axial dispersion. Since the pressure drop measured along the reactor was always below 10% the absolute pressure, no momentum balance was solved. The material balance was solved using the differential Equation (5):

$$\frac{\partial \dot{n}}{\partial m_{\text{cat}}} = r_{m,i} = \sum_j v_j r_{m,j} \quad (5)$$

Beside the material balance, an energy balance was solved for the heat exchanger-reactor, since all the kinetic constants are temperature dependent and assumption of an isothermal bed can induce error in

data evaluation. In this regard, all the temperatures i.e. gas temperature in the inlet of the reactor, cooling air and the reactor body were adjusted by electrical heating to the actual setpoint. The catalyst bed temperature is measured with the internal thermocouples. The solved energy balance (Equation (6)) includes the convective heat transport in axial direction, the released reaction heat, and the heat transfer from the catalyst bed of the reaction zone towards coolant air into account.

$$\frac{\partial T}{\partial m_{\text{cat}}} = \frac{1}{\sum_i \dot{n}_i C_{p,i}} \left(- \sum_j r_{m,j} \Delta_R H_j - \alpha_c U \frac{L_{\text{bed}}}{m_{\text{cat}}} (T - \bar{T}_c) \right) \quad (6)$$

The heat transfer coefficient α_c includes all the transfer resistances between the reaction zone and the cooling channel. The value of the coefficient is taken from [29], in which the same reactor concept has been applied. This coefficient is tuned regarding the experimental observations made through the inserted thermocouples in comparison to the temperature setpoint. The temperature in catalyst bed is considered gradient-free in width and height direction. For the cooling temperature, the average of inlet and outlet values of air temperature (\bar{T}_c) are used due to low difference of experimental values. On the other hand, the local increase in the temperature of the air is calculated in the model by considering no losses to the environment. The numerical calculation of material and energy balances was carried out in Matlab® applying ode15s as the solver.

The modeled length dependent temperature in the reactor for the temperature setpoint of $300\text{--}450\text{ }^\circ\text{C}$ at $p_{\text{abs}} = 4\text{ bar}$ and $\tau_{\text{mod}} = 0.38\text{ mg}_{\text{cat}}\text{ min Nml}_{\text{CO}_2}^{-1}$ is provided in Fig. 2 while the corresponding experimental values are provided in Table 2. Position 1 (marked as P1 in Fig. 1) refers to the thermocouple which measures

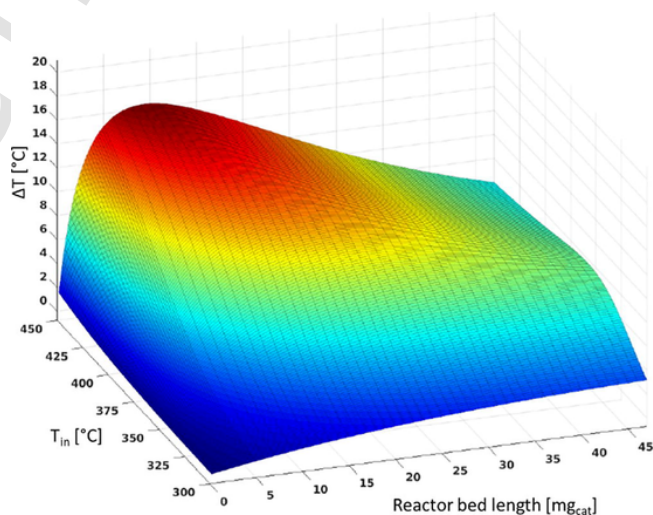


Fig. 2. The modeled temperature profile as function of the catalyst bed length for temperature setpoints of $300\text{--}450\text{ }^\circ\text{C}$, $p_{\text{abs}} = 4\text{ bar}$ and $\tau_{\text{mod}} = 0.38\text{ mg}_{\text{cat}}\text{ min Nml}_{\text{CO}_2}^{-1}$.

Table 2

Experimental temperatures near the catalyst bed at half of the bed length at temperature setpoints of $300\text{--}450\text{ }^\circ\text{C}$, $p_{\text{abs}} = 4\text{ bar}$ and $\tau_{\text{mod}} = 0.38\text{ mg}_{\text{cat}}\text{ min Nml}_{\text{CO}_2}^{-1}$.

$T_{\text{in}} [^\circ\text{C}]$	T in position 1 [$^\circ\text{C}$]	T in position 2 [$^\circ\text{C}$]
300	300	301
320	320	322
335	335	341
350	350	356
385	385	392
400	401	408
450	452	458

the temperature at half of the bed length near the catalytic bed on the inlet side of the cooling air, while position 2 is measured at the same bed length but on the outlet side of the cooling air (marked as P2 in Fig. 1).

2.4.3. Parameter estimation and statistical evaluation

The parameters of different tested models were estimated by solving a minimization problem. For that, the sum of least square residuals (RSS) of carbon-containing species yield (CO_2 , CO and CH_4) were defined. Nonlinear regression was the preferred analysis method for determination of the kinetic parameters, applying an iterative search procedure [30]. Minimization was done applying the `lsqnonlin` function and Levenberg-Marquardt algorithm in MATLAB®. By each iteration of the `lsqnonlin` function, the kinetic parameters were estimated, and the square error RSS value was calculated.

For evaluation of the fit between the model and experimental data, the adjusted coefficient of determination R^2_{adj} was compared. This parameter is a modified linear coefficient of determination R^2 that also takes the number of parameters in a complex model into account. It allows to judge the necessity of applying more parameters for improving the description of the experimental data. The maximum value for R^2_{adj} is one, which corresponds to a perfect consistency between the data points and the model. In contrast to R^2 , the value of R^2_{adj} can also be negative which indicates the model has too many parameters [31]. In this work, for each carbon-containing species CO , CO_2 and CH_4 an individual R^2_{adj} was calculated to assess the accuracy of different models with regard to selectivity.

Discrimination among several competing models with different number of parameters was accomplished applying Bayesian information criterion (BIC) proposed by Schwarz [32]. For BIC calculation, the maximum likelihood function, the number of independently adjusted parameters within the model and the number of the data-points are required. In a simplified form of this criterion and under the assumption that the model errors and disturbances are independent and identically distributed, the sum of squares of the residuals (RSS) can be replaced by the maximum likelihood function, developed by Akaike and inspired by Schwarz [33]. When comparing two models, the one having lower value of BIC is preferred. A lower BIC value indicates either fewer variables, better fit, or both.

To evaluate the accuracy and reliability of the model parameters, a confidence interval of 95% for each estimated parameter was defined. Finally, to evaluate how strongly two parameters are correlated to each other the correlation matrix was determined as specified in [31].

3. Results and discussion

3.1. Development of the kinetic model

As explained in Section 2.4.1, the rate equations tested in this work are based on a LHHW model. The general form of the tested equation for the two reactions of interest is as:

$$r_{(rWGS)} = \frac{k_1 p_{\text{CO}_2}^\alpha p_{\text{H}_2}^\beta}{\text{inhibition term}^2} \left(1 - \frac{p_{\text{CO}} p_{\text{H}_2} \text{O}}{p_{\text{CO}_2} p_{\text{H}_2} K_{rWGS}}\right) \quad (7)$$

$$r_{(\text{CO-Methanation})} = \frac{k_2 p_{\text{CO}}^\gamma p_{\text{H}_2}^\phi}{\text{inhibition term}^2} \left(1 - \frac{p_{\text{CH}_4} p_{\text{H}_2} \text{O} p_{\text{abs}}^2}{p_{\text{CO}} p_{\text{H}_2}^3 K_{\text{CO-Meth}}}\right) \quad (8)$$

The reaction rate models are derived from postulations on the reaction mechanism, therefore values of zero, 0.5 and 1 are proposed for

the reaction orders (here: α , β , γ , ϕ), whereas the value 1 stands for a direct adsorption and 0.5 for a dissociative adsorption on the surface. CO can also adsorb in the bridged mode on the surface of Ni catalyst. However according to literature, this adsorption mode is a much more stable conformation and is associated with a poisoning influence on the Ni surface and cannot be effectively hydrogenated [34,35] and is thus not considered here. Zero was also a possible value which would mean that this species has no influence on the reaction rate. In this work, combinations of these values for the reactant exponents were used:

$$\left(\frac{\alpha =}{0; 1/2; 1}\right) \times \left(\frac{\beta =}{1/2; 1}\right) \times \left(\frac{\gamma =}{0; 1/2; 1}\right) \times \left(\frac{\phi =}{1/2; 1}\right) \quad (9)$$

Based on the experimental observation (see 3.3.2) an exponent of zero for hydrogen was considered infeasible and therefore not used for parameter estimations. The method of least squares as described in Section 2.4.3, proved that $\alpha = 0.5$, $\beta = 0.5$, $\gamma = 1$ and $\phi = 0.5$ yielded the most suitable reaction orders.

The inhibition term of the model was assessed both experimentally (see sections 3.3.3 and 3.3.4) and with modelling. The reaction hindrance by CO and/or H_2 was considered a plausible scenario considering the high affinity of Ni catalyst to CO . H_2 could be adsorbed on the catalyst surface in molecular and dissociative way.

$$\left(\frac{v_{\text{H}_2} =}{0; 1/2; 1}\right) \times \left(\frac{v_{\text{CO}} =}{0; 1}\right) \quad (10)$$

The modelling results indicated that inhibition by CO and/or H_2 does not help to reduce the RSS value. For most of the combinations the adsorption constant was rather close to zero and therefore CO and H_2 were confirmed to have no inhibiting effect. Hindrance by CO_2 was considered only relevant for rWGS reaction. Since the RSS value was observed to increase with a factor of 10 when applying CO_2 in the inhibition term, the hindrance was rejected. The experimental tests on CO , H_2 and CO_2 influence on CO_2 methanation and rWGS reactions are presented in 3.3.4 and are in accordance with the modelling results.

The mathematical feasibility of inhibition of the reaction by the products was assessed by testing two terms for CH_4 : no adsorption and simple adsorption, and four terms for water: 1. no adsorption, 2. direct adsorption, 3. adsorption as a hydroxyl group and 4. adsorption as oxygen on the catalyst surface.

$$\left(\frac{\text{Inhibition by } \text{CH}_4 =}{0; K_{\text{CH}_4} p_{\text{CH}_4}}\right) \times \left(\frac{\text{Inhibition by } \text{H}_2\text{O} =}{0; K_{\text{H}_2\text{O}} p_{\text{H}_2\text{O}}; K_{\text{OH}} \frac{p_{\text{H}_2\text{O}}}{p_{\text{H}_2}}; K_{\text{O}} \frac{p_{\text{H}_2\text{O}}}{p_{\text{H}_2}}}\right) \quad (11)$$

Without an inhibition term (resulting in a simple power rate law) the model was unable to reflect the conversions over 60%, as already found by Koschany et al. [18]. When only CH_4 was considered in the inhibition term, the higher conversion regime could be modelled, but not the effect of water addition in the feed (see section 3.3.3). Combinations of CH_4 and water inhibition delivered only values close to zero for the methane adsorption constant (K_{CH_4}). Therefore, water was conceived as the only factor inhibiting the reaction progress. In contrast to literature models, in which water has been mainly modeled as oxygen or hydroxyl groups on the catalyst surface [18,19], in this study a simple water adsorption resulted in the best fit. The final model identified as the most suitable and used to describe the reaction experimental data is provided in Equation (12) and Equation (13):

$$r_{(rWGS)} = \frac{k_1 P_{CO_2}^{0.5} P_{H_2}^{0.5}}{DEN^2} \left(1 - \frac{P_{CO} P_{H_2O}}{P_{CO_2} P_{H_2} K_{rWGS}} \right) \quad (12)$$

$$r_{(CO-Meth)} = \frac{k_1 P_{CO} P_{H_2}^{0.5}}{DEN^2} \left(1 - \frac{P_{CH_4} P_{H_2O} P_{abs}^2}{P_{CO} P_{H_2}^3 K_{CO-Meth}} \right) \quad (13)$$

The inhibition term is defined as:

$$DEN = 1 + K_{H_2O} P_{H_2O} \quad (14)$$

The reaction rate and adsorption constants are employed with Arrhenius and Van't Hoff approach:

$$k_i = k_{555K,i} \exp\left(\frac{E_{A,i}}{R} \left(\frac{1}{555K} - \frac{1}{T}\right)\right) \quad (15)$$

$$K_{H_2O} = K_{H_2O,555K} \exp\left(\frac{\Delta H_{H_2O}}{R} \left(\frac{1}{555K} - \frac{1}{T}\right)\right) \quad (16)$$

The fit used for the equilibrium constants of rWGS reaction and CO methanation is as follows:

$$K_{rWGS} = \frac{1}{10^{-2.4198 + 3.855 \times 10^{-4} T + \frac{2180.9}{T}}} \quad (17)$$

$$K_{CO-Meth} = 10^{4.1002 \times 10^{-5} T^2 - 0.080257 T + 39.6039} \quad (18)$$

The estimated parameters and their 95% confidence intervals are given in Table 3. The confidence intervals for all parameters are relatively small, except for water adsorption enthalpy.

Table 4 shows the correlation matrix of the used parameters. Half of the values are in the range of 0 to 0.5. A quarter of the values are between 0.5 and 0.65 and the rest are between 0.65 and 0.75. Since all the correlation values are well below 0.9 the parameters display very low correlation to each other and overall it is concluded that although there are some moderate dependencies, all parameters are well-defined and have their own explicit function in the model.

Table 3

Parameter estimation for the rWGS (1) and CO methanation (2) reaction rate models and their corresponding 95% confidence interval.

Parameter	Value	unit	Confidence interval 95%
$K_{1, 555 K}$	0.1435	mol (kg s bar) ⁻¹	±0.02994
$E_{A, 1}$	166.55	kJ mol ⁻¹	±8.48
$K_{2, 555 K}$	11.5451	mol (kg s bar ^{1.5}) ⁻¹	±0.7854
$E_{A, 2}$	60.98	kJ mol ⁻¹	±4.59
$K_{H_2O, 555 K}$	0.6782	bar ⁻¹	±0.03763
ΔH_{H_2O}	11.44	kJ mol ⁻¹	±4.96

Table 4

Correlation matrix of the parameters in the suggested model.

	$K_{1, 555 K}$	$K_{2, 555 K}$	$K_{H_2O, 555 K}$	$E_{A, 1}$	$E_{A, 2}$	ΔH_{H_2O}
$K_{1, 555 K}$	1					
$K_{2, 555 K}$	-0.554	1				
$K_{H_2O, 555 K}$	0.474	-0.745	1			
$E_{A, 1}$	0.127	-0.082	-0.403	1		
$E_{A, 2}$	-0.540	0.660	-0.412	-0.530	1	
ΔH_{H_2O}	-0.003	0.222	0.054	-0.686	0.669	1

Table 5

Statistical comparison of the new two-step CO₂ methanation rate model with literature models.

Model	BIC	RSS	R ² _{adj} (CO ₂)	R ² _{adj} (CH ₄)	R ² _{adj} (CO)
Koschany [18]	-426.463945	9.94	0.8909	0.8322	-
Zhang [20]	-371.328814	12.25	0.8516	0.7548	0.4236
Kopyscinski [19]	-379.522865	11.66	0.8363	0.7735	-0.0151
Our new suggested model	-636.658778	2.98	0.9266	0.8888	0.4832

3.2. Comparison to literature models

The sum of squares of the residuals of the yield of carbon containing species $RSS(Y_{c,i})$ as well as the adjusted coefficient of determination R^2_{adj} between modelled and experimentally observed volumetric flow rates of CO₂, CH₄ and CO at the reactor exit were used for evaluation of the three literature models versus the developed model (see Table 5). The RSS values for all three literature models after being fitted to our experimental data are up to a factor of three higher than for our model. This is a first indication of better description of the experimental data with our recommended model. The R^2_{adj} (CO₂) for all the literature models is below 0.9, whilst the new model reaches a value of 0.93 which is the closest to one. For the case of CH₄, the R^2_{adj} is equal to 0.89 and is superior compared to other models as well. An improvement in R^2_{adj} (CO) can be grasped compared to Zhang's model with 0.42 versus 0.48 for our model. The model of Kopyscinski resulted in a negative value in R^2_{adj} (CO) and for Koschany's model no R^2_{adj} (CO) could be estimated, since it does not consider CO formation at all. The negative value for R^2_{adj} indicates that this model cannot be applied for specifying CO methanation as an intermediate step and may be an indication of too many parameters.

In conclusion, the model of Koschany, which applied the same reaction exponents as in this work, can simulate the CH₄ and CO₂ product flow rates best amongst the literature models. The model of Zhang, nevertheless, was the only proper literature model for simulating CO formation as intermediate.

Another advantage of the current model is reflected by the BIC factor. The new model has the smallest value (highest negative number). The modest number of the parameters used in this model together with accurate description of the formation/consumption of species led to this favorable BIC. Therefore, it is confirmed that 6 applied parameters are advantageous in comparison to complex models of Kopyscinski and Zhang, in which 12 parameters are applied.

The activation energy of the CO methanation reaction in this work is calculated to be 61 kJ mol⁻¹ as indicated in Table 3. Kopyscinski estimated a value of 74.1 kJ mol⁻¹. Also, the other works report similar values: Gardner und Bartholomew 72–78 kJ mol⁻¹ [36], McCarty und Wise 71 kJ mol⁻¹ [37] und Hayes et al. 78 kJ mol⁻¹ [38]. The possible reason for lower activation energy calculated in this work can be explained by the change of the active site from Ni in literature studies to Ni₃Fe catalyst in our study. The activation energy of the rWGS reaction via our developed model was determined as 166.6 kJ mol⁻¹. In literature a wide spectrum of values for WGS reaction (opposite reaction pathway) on diverse catalysts are reported [39,40]. For the Ni/Al₂O₃ catalysts literature values of about 85 kJ mol⁻¹, while for Fe-Oxide catalyst about 150–160 kJ mol⁻¹ are reported. The fitted models of Zhang and Kopyscinski provided 108 kJ mol⁻¹ and 202 kJ mol⁻¹ respectively. Therefore, the estimated activation energy for rWGS by our model for Ni₃Fe catalyst seems physically meaningful as the value is in the middle of the whole spectrum.

Some features of the new model against the literature models can be best compared when having a closer look on conversion and selectivity dependence on temperature, as plotted in Fig. 3. The experimental data points are marked with their corresponding standard deviation bar that is calculated as clarified in section 2.3. The standard deviation for the reference equals to 2.74% and the relative standard deviation is estimated to be 4.7%. The predications made by the literature models are presented with newly fitted parameters, since they failed completely to describe the trends of the Ni_3Fe catalyst used in this work. As it is evident in Fig. 3 left, in all the models the conversion increases with increasing the temperature according to the Arrhenius law. Afterwards, the conversion approaches a plateau, which can be argued through several causes: 1. Inhibition by the reaction products, 2. reaching the equilibrium and 3. transport limitations. The first two are reflected in the developed model, and hence the model can simulate this behavior with temperature increase. The possibility of transport limitations is already ruled out as mentioned in 2.3. The developed model displays the smallest deviation among all. Its trend look similar to the one simulated with Koschany's model. This similarity can be explained with the fact that the same reaction order in both models were applied. However, Koschany overestimates the conversion in the temperature range of 330 °C up to 450 °C and the equilibrium is already reached at lower temperature. At higher conversions, the product inhibition plays obviously a more important role than predicted by the Koschany model. The different form of inhibition term of the developed model compared to that of the Koschany model suggested, helps to avoid overestimation. The models of Zhang and Kopyscinski fit the data only in the middle temperature range (350–400 °C). In the high and low conversion region, they both overestimate the conversion. The model of Kopyscinski crosses the thermodynamic equilibrium conversion at 430 °C, which is clearly due to neglecting the thermodynamic term in the CO-methanation model and emphasizes on the importance of integrating this term in the model.

Fig. 3 right shows that the lowest selectivity measured is 95% at 300 °C. It reaches a maximum of 98% at 350 °C and decreases to 97% at higher temperatures. Our model simulates the trend of maximum evolution between 335 °C and 425 °C; however, it still underestimates the selectivity especially in the lower temperature range ($T < 320$ °C). The models of Zhang and Kopyscinski simulate a positive trend for increasing selectivity with increasing temperature which is not the case as the experimental data indicate. The model of Zhang exhibits only a small maximum at 430 °C due to equilibrium and the Kopyscinski model misses such trend completely. The model of Koschany cannot be applied for selectivity prediction, since it simulates direct CO_2 methanation.

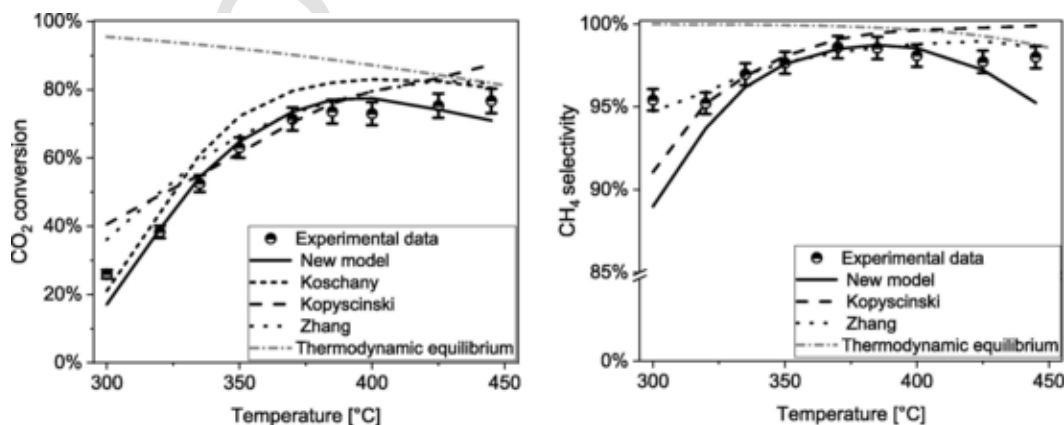


Fig. 3. Comparison of the CO_2 conversion (left) and CH_4 selectivity (right) as function of temperature for experimental data to the developed model and the literature models ($p = 4$ bar, $\tau_{\text{mod}} = 0.72 \text{ mg}_{\text{cat}} \text{ min Nml}_{\text{CO}_2}^{-1}$).

3.3. Influence of experimental conditions on reaction rate

3.3.1. Temperature

For better discussion of the observed effects on intermediate CO formation, the yield of CO formation over CO_2 conversion for different temperatures is plotted in Fig. 4. For 300 °C only small amounts of CO were formed and the maximum value for CO yield is only 2%. At higher temperatures (350 °C and 400 °C) much higher CO yield (up to 7%) can be observed; by increase in CO_2 conversion ($>70\%$) the CO yield drops quickly to below 2%. The propagation of the of Y-X curve for $T = 300$ °C with local maxima suggests that CO is the intermediate between CO_2 and CH_4 . At $T > 350$ °C, when the required residence time is much shorter, substantial amounts of generated CO are measured at intermediate CO_2 conversions. By increasing the residence time, CO_2 conversion improves and therefore CO intermediate reacts also further to CH_4 . In between the two temperatures of 300 °C and 350 °C, there is a continuous transition, indicated by data collected at 335 °C, which connects the low-temperature-regime to high-temperature-regime. Having a look on the estimated values for rWGS and CO methanation in Table 3 illustrates that the activation energy for rWGS reaction is much higher than for the CO methanation (166.55 versus 60.98 kJmol^{-1}). That means the rWGS reaction gets faster compared to CO methanation at higher temperature. As Fig. 4 illustrates, this transition is simulated accurately with our recommended model.

3.3.2. H_2/CO_2 ratio

The H_2/CO_2 ratio was varied from 2 to 8 with two different measurement series as already clarified in section 2.3. In all measurements, the modified residence time for CO_2 was kept constant ($=0.38 \text{ mg}_{\text{cat}} \text{ min Nml}_{\text{CO}_2}^{-1}$) in order to make solid conclusions on the integral consumption of species. The influence of H_2/CO_2 variation on CH_4 selectivity is completely different for the two studied scenarios. Thus, for better understanding of the involved effects on reaction rate in the H_2/CO_2 variation tests, CH_4 selectivity in the experiment of p_{H_2} variation is also compared with experiments where total pressure was varied in constant ($=4$) H_2/CO_2 ratio. CO_2 and H_2 conversion and CH_4 selectivity in dependence of the varied p_{H_2} are plotted in Fig. 5 (left: CO_2 and H_2 conversion, right: CH_4 selectivity). Fig. 5 (left) exhibits that in the beginning H_2 conversion is constant ($\sim 60\%$, $p_{\text{H}_2} = 0.8\text{--}1.6$ bar), where CH_4 selectivity is considerably rising from its lowest level ($=91\%$, Fig. 5 right) with increasing p_{H_2} . With further increase in p_{H_2} ($p_{\text{H}_2} > 2$ bar), H_2 conversion starts to drop with an accelerating trend. Such behavior can be interpreted that in lower p_{H_2} region, the added H_2 is consumed instantaneously to products with overall increasing rate. At $p_{\text{H}_2} > 1.6$ bar, the stoichiometry is reached and

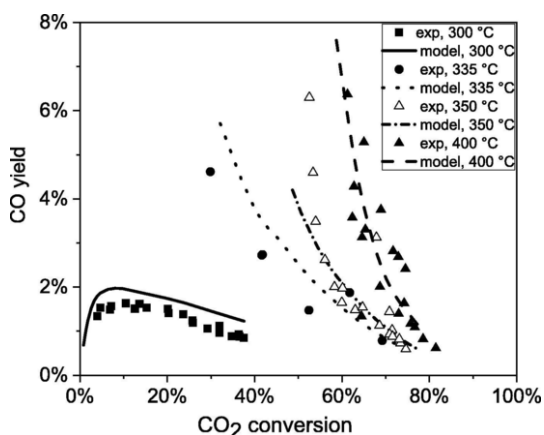


Fig. 4. Y_{CO} - X_{CO_2} diagram for CO formation from CO_2 derived from different temperatures, modified residence time and pressures.

additional dosed H_2 remains unreacted, which leads to a H_2 conversion drop. According to Fig. 5 (left), CO_2 conversion has a positive trend in the whole range of p_{H_2} increase, so that more CO could appear through rWGS reaction. However, further conversion of CO to methane is rather depending on H_2 concentration and not on CO_2 amount present (see 3.3.4), so with higher H_2 concentration, its conversion to CH_4 is guaranteed and that explains the enhancing trend for CH_4 selectivity in Fig. 5 (right). The CH_4 selectivity for data with constant $H_2/CO_2 = 4$ has exact same trend as when CO_2 is kept constant. Since the increased

methane selectivity (Fig. 5 right) and the increased CO_2 conversion (Fig. 5 left) have very similar trends, an identical reaction order is plausible for CO_2 and H_2 in both, the rWGS and the CO methanation reaction.

Fig. 6 depicts the results of the case where p_{H_2} is kept at 1.6 bar and p_{CO_2} is varied. In Fig. 6 (left), CO_2 conversion shows a linear drop with increasing p_{CO_2} and extra dosed CO_2 remains unreacted. Even though the graph starts at over-stoichiometric H_2 -conditions this trend is continuously valid over the whole range of p_{CO_2} which leads us to the assumption that the surface is already saturated with CO_2 species. On account of the CO_2 saturated surface, the produced CO through rWGS reaction should also stay constant. As p_{H_2} is kept constant, the following CO methanation reaction has also a constant rate, which is supported from the finding of a constant selectivity in CH_4 formation (Fig. 6 right). Experimental points with $H_2/CO_2 = 4$ prove this argument, in which for example for the data points with $p_{H_2} < 1.6$ bar ($p_{CO_2} < 0.4$ bar) the methane selectivity is lower than the corresponding points with $p_{H_2} = 1.6$ bar = const (92% versus 96%). When $H_2/CO_2 < 4$ (and so $p_{CO_2} > 0.4$ bar), the CH_4 selectivity stays below that of the stoichiometric data points (97.8% versus 96%). This confirms that the CO_2 concentration has no influence on selectivity in the product distribution and on the CO methanation reaction.

3.3.3. Water addition

The effect of adding water in the feed is depicted in Fig. 7 (left). After adding 10 vol% water in the feed, the conversion drops from 23% to 9%. By further increase of the water flow rate, the conversion drops further. The experiment proves that water has a significant retarding

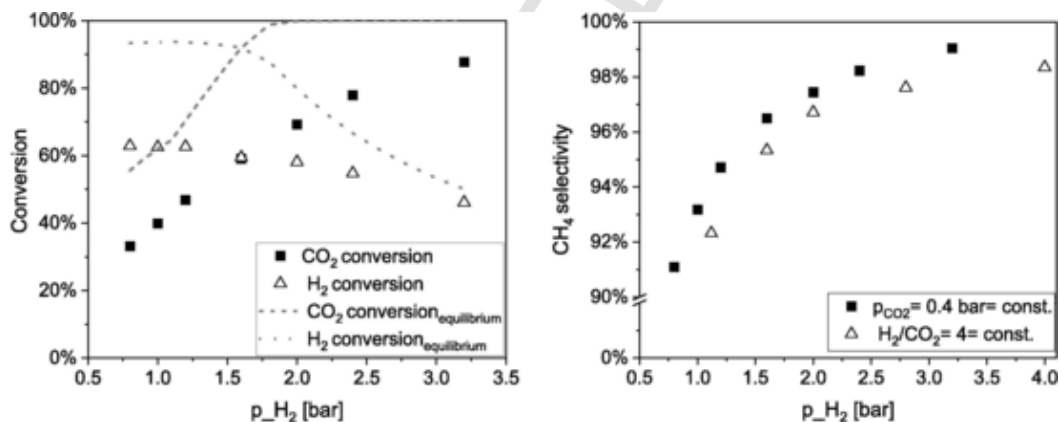


Fig. 5. CO_2 and H_2 conversion (left) and CH_4 selectivity (right) in dependence of the H_2 partial pressure ($p_{CO_2} = 0.4$ bar = const., $T = 350$ °C, $\tau_{mod} = 0.38$ mg_{cat} min Nml_{CO₂}⁻¹). In the right figure a plot of CH_4 selectivity is added for variation of total pressure at $H_2/CO_2 = 4 =$ const. ($T = 350$ °C, $\tau_{mod} = 0.38$ mg_{cat} min Nml_{CO₂}⁻¹).

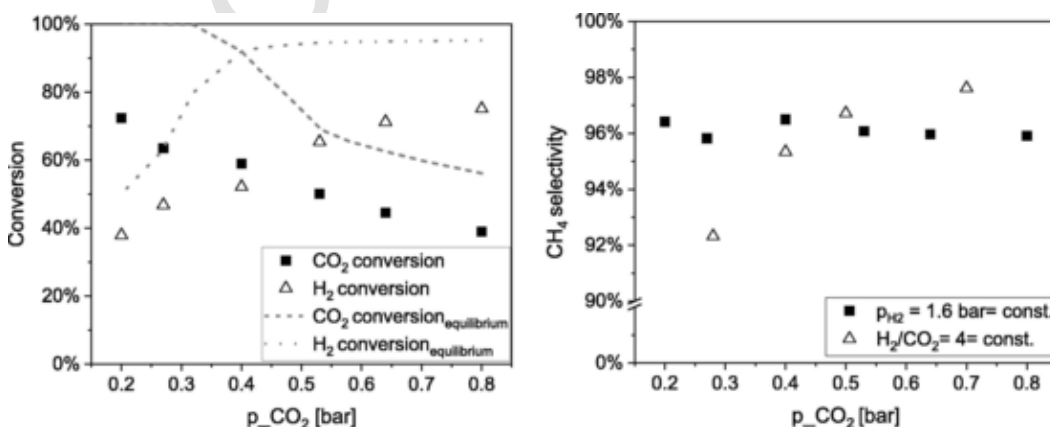


Fig. 6. CO_2 and H_2 conversion (left) and CH_4 selectivity (right) in dependence of the CO_2 partial pressure ($p_{H_2} = 1.6$ bar = const., $T = 350$ °C, $\tau_{mod} = 0.38 =$ mg_{cat} min Nml_{CO₂}⁻¹). In the right figure a plot of CH_4 selectivity is added for variation of total pressure at $H_2/CO_2 = 4 =$ const. ($T = 350$ °C, $\tau_{mod} = 0.38$ mg_{cat} min Nml_{CO₂}⁻¹).

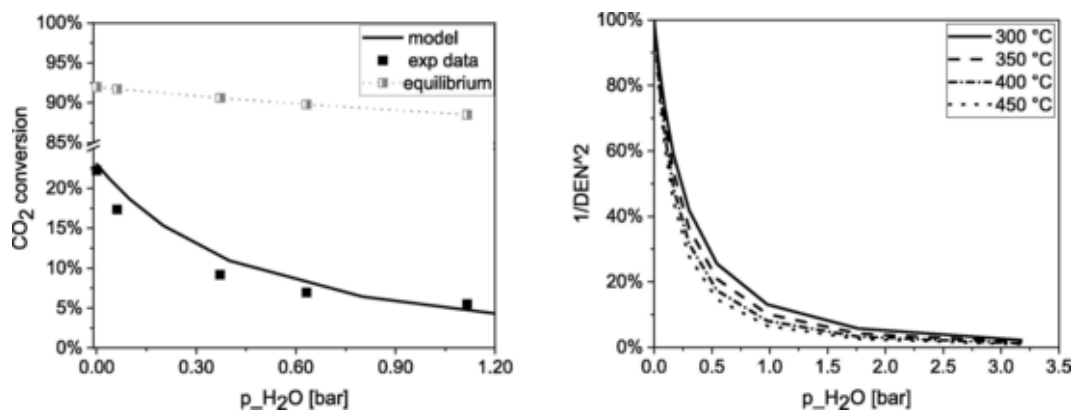


Fig. 7. Influence of water addition on CO₂ conversion at T = 350 °C, $\tau_{\text{mod}} = 0.38 = \text{mg}_{\text{cat}} \text{ min Nml}_{\text{CO}_2}^{-1}$ and p = 4 bar together with corresponding thermodynamic conversion at corresponding operational condition(left), illustration of the inhibiting effect of water through inhibition term in different temperatures as a function of water pressure (right).

impact on the reaction rate, which, as given in Equation (13), is included in the rate equation through the water adsorption term. Fig. 7 left exhibits that the model for different water concentrations added in feed precisely simulates the rate drop.

In this context, the value of inhibition term is calculated for different temperature and water partial pressures and plotted in Fig. 7 (right). When no water is present in the gas mixture, DEN approaches 1, and the reaction rate is not affected. By adding small amounts of water in the feed, the rate decreases sharply. For example, for p_{H₂O} = 0.2 bar, the reaction rate is reduced to about 50% of its initial value. The plot indicates that this reduction is weakly temperature dependent. Fig. 7 reveals further that the conversion drop during water partial pressure increase (left plot) has the exact trend as the inhibition term (right diagram). This proves that reduction in conversion in presence of water is not affected by rWGS reaction equilibrium, but explicitly from presence of water in the reacting mixture.

Several literature works have reported the inhibiting effect of water on the rate of methanation reaction [19]. Theofanidis et al. [41] have shed some light on most important mechanistic concerns of CO₂ activation on Ni-Fe catalyst. Based on their study, CO₂ is dissociated on the Fe sites to surface CO and iron oxide (Equation (19)). It is well known that H₂ is strongly attracted by Ni and adsorbs dissociative on a Ni surface [42]. Through an alternating pulse experiment over Fe promoted Ni catalyst they could show that a redox reaction occurs, in which H₂ reduces the oxidized Fe sites (Eq. (20)).

A possible explanation for the inhibition effect of water observed in our experiments is that, by increasing the water concentration, the CO₂ activation sites are blocked with water leading to a competing adsorption of water and CO₂ over the free sites. Furthermore, water can ad-

sorb on the oxidized iron sites and can compete with hydrogen to reduce iron, thus, the rate of CO₂ conversion is slowed down.



3.3.4. CO/CO₂ addition

The experimental results of the CO/CO₂ mixture methanation are always reported as consumed amount of the CO and CO₂ to provide an integral reaction rate. In addition, it is impossible to calculate the CO conversion and the methane selectivity explicitly from CO₂. Only the CO consumption and formation can be discussed with balance equations and comparison to a reference point. In Fig. 8 (left) the results of converted CO and CO₂ in Nml min⁻¹ are shown for different flows of CO (0–11.4 Nml min⁻¹) added in the feed. By increasing the CO amount from 0 to 11.4 Nml min⁻¹, the CO₂ consumption decreases from 64 Nml min⁻¹ to 61 Nml min⁻¹. It may seem that CO can have a slightly negative influence on CO₂ consumption. However, it can also be due to thermodynamic equilibrium, the additional H₂ consumption or inhibition due to extra water produced from the added CO. Since the model describes the experimental data accurately (the solid line in Fig. 8 left), it is concluded that no further CO inhibition term for the rWGS reaction is necessary and water serves as the only retarding species. Another interesting conclusion made from this experiment is that the CO methanation rate is not influenced by CO₂ in the feed, since the values for CO consumption in the case of mixed methanation and pure CO methanation (dotted line, Fig. 8 left) lay on a straight line with an identical slope.

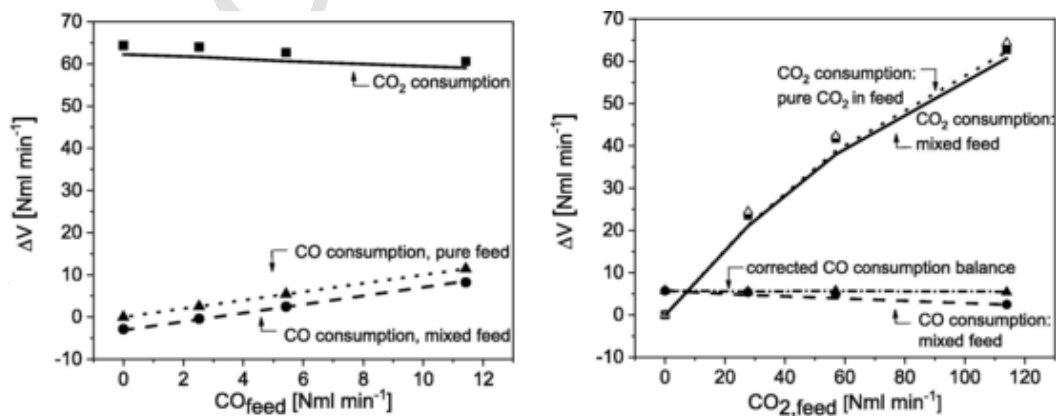


Fig. 8. Variable CO addition in constant CO₂ volumetric flow rate influence on CO and CO₂ consumption (left), variable CO₂ addition in constant CO volumetric flow rate influence on CO and CO₂ consumption (right).

Fig. 8 (right) demonstrates the changes in reactants consumption in variable CO_2 in the feed ($0\text{--}115 \text{ Nml min}^{-1}$) with constant CO (6 Nml min^{-1}) added to the feed. The first impression might be that CO consumption reduces with increasing the CO_2 flow rate in the feed (dashed line, Fig. 8 right). Therefore, the four experiments of CO_2 flow rate variation, this time without CO in the feed were performed (pointed line, Fig. 8 right), to add the CO formed from CO_2 in the balance. It can be seen that the CO consumption remains constant and equals 5.6 Nml min^{-1} . Thus, the reaction hindrance due to CO_2 addition in the CO methanation rate can be ruled out. This result is coherent with the observations made in varied H_2/CO_2 ratio (section 3.3.2). In this test, reacted CO_2 is only slightly influenced by the added CO and the deviation is less than 3%. This difference can be due to the increased H_2 consumption, thermodynamic effects or additionally formed water from the added CO, which is also correctly reflected by the model (solid and pointed lines, Fig. 8 right).

3.4. Evaluation of the developed model

The consistency between the experimental data and the model can be further analyzed with parity plots (see Fig. 9). The calculated volumetric flow rates at the reactor exit applying the kinetic rate model is compared versus the experimentally measured values for all the 166 experimental data points. Major share of the data are in the range of $\pm 25\%$ between the model and the measured points. The careful evaluation of the data shows that the inconsistent points are mainly in the smaller flow rates ($< 100 \text{ Nml min}^{-1}$). The data points corresponding to CO concentrations have the highest scattering of all. However, there is no systematic error recognizable in the CO parity plot and the scattering seems to have a statistical nature. The CO concentrations in the product gas were always much smaller compared to CO_2 and CH_4 , ($0.1\text{--}1\%$ compared to $10\text{--}20\%$ and/or $1\text{--}15 \text{ Nml min}^{-1}$ vs. $20\text{--}500 \text{ Nml min}^{-1}$) which result in a larger standard deviation and thus larger scattering.

4. Conclusion

Motivated by technical progress in Power-to-Gas processes and the required dimensioning of new short-contact-time reactors, CO_2 methanation reaction kinetics is studied in a cross flow cooled microstructured packed bed reactor using a Ni_3Fe catalyst [21]. The process parameters of temperature, pressure, residence time and composition of the reactants were varied. The measured conversion and selectivity were used for evaluation of literature models and development of a new model for a consecutive CO_2 methanation pathway with less parameters.

The reactor model implemented was a 1-D non-isothermal pseudo-homogeneous model. The modeling of the reaction was carried out

based on Langmuir-Hinshelwood formalism. The mathematical terms were picked systematically based on experimental observations as well as literature results published by Koschany, Kopyscinski and Zhang [18–20]. The model with the smallest sum of least square residuals was chosen. Its qualities were confirmed using different criteria such as confidence interval of the parameters, correlation matrix and adjusted coefficient of determination R^2_{adj} . The evaluation of different aspects revealed that our developed model based on two-step CO_2 methanation with direct water adsorption in the inhibition term provides the smallest sum of least square residuals and the best agreement to the experimental data. In this context, no postulations on the reaction mechanism on Ni_3Fe catalyst can be provided. The validity of the calculated parameters was confirmed by comparing them to relevant literature data and it could be confirmed that the recommended model provides an enhanced description of the reaction with a lower number of parameters.

The selectivity to methane formation was shown to be strongly dependent on temperature and residence time. Shorter residence time and higher temperatures favor CO formation. Especially between $320 \text{ }^\circ\text{C}$ and $350 \text{ }^\circ\text{C}$, the yield of CO increases strongly. This selectivity behavior could be enlightened through describing the methane formation from CO_2 as a two-step reaction: the reverse water gas shift followed by CO methanation. In this regard, CO is the intermediate of the reaction and its abundant yield at higher temperatures and lower residence times was explained by the notably higher activation energy of reverse water gas shift reaction compared to CO methanation (167 KJ mol^{-1} vs. 61 KJ mol^{-1}) computed in this work. Stoichiometric variation of the reactants provided solid proof that CO_2 concentration has no influence on the rate of CO methanation reaction and that H_2 possibly has a similar order in both reactions. The experiments with CO addition in the feed (with and without CO_2) demonstrated that CO and CO_2 have no retarding effect on reaction rate. The reaction rate hindrance due to water formation was confirmed experimentally through addition of water in the feed mixture. It was shown that this effect is rather less dependent on temperature and that the water concentration is the main inhibiting factor.

Acknowledgment

Funding of this research by the by the German Ministry for Education and Research (BMBF) within the KOPERNIKUS Project Power2X (P2X) under contract No. 03SFK2K0 is gratefully acknowledged.

The authors gratefully acknowledge the support of Prof. Dr. Jan-Dierk Grunwaldt and Marc-André Serrer for providing the Ni_3Fe catalyst applied in this study.

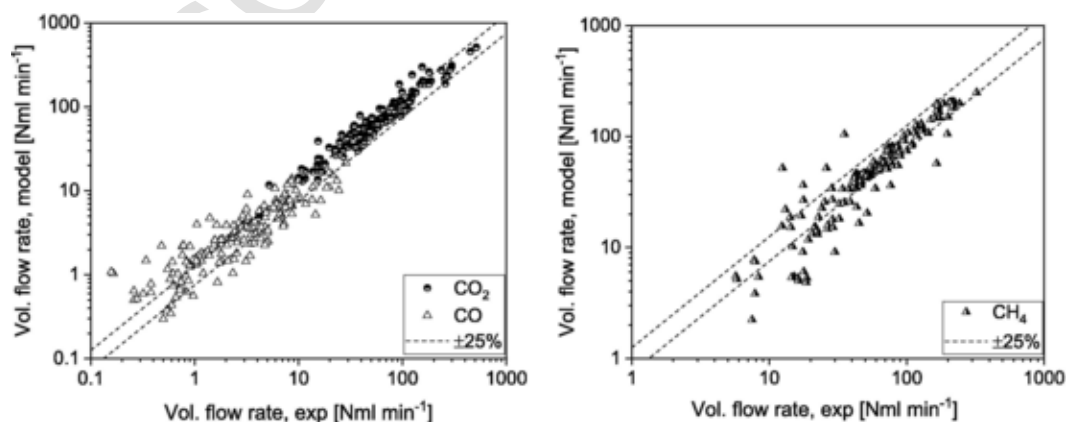


Fig. 9. Parity plots for comparison of the experimental data to the recommended LHHW rate model for CO and CO_2 volumetric flows (left), and CH_4 volumetric flow (right).

References

- [1] M. Sterner, I. Stadler, *Energiespeicher - Bedarf, Technologien, Integration*, Springer Berlin Heidelberg, Berlin, Heidelberg, 2017.
- [2] V. Quaschnig, *Regenerative Energiesysteme: Technologie - Berechnung - Simulation*, Hanser, München, 1998.
- [3] N. Nuttall, *Historic Paris Agreement on Climate Change: 195 Nations Set Path to Keep Temperature Rise Well Below 2 Degrees Celsius*, 2015, <https://unfccc.int/news/finale-cop21>, accessed 1 August 2019.
- [4] P. Sabatier, J.B. Senderens, *New methane synthesis*, C. R. Acad. Sci. Paris 314 (1902) 514.
- [5] S. Fendt, A. Tremel, M. Gaderer, H. Spliethoff, *The potential of small-scale SNG production from biomass gasification*, *Biomass Conv. Bioref.* 2 (2012) 275–283.
- [6] S. Rönsch, M. Kaltschmitt, *Bio-SNG production – concepts and their assessment*, *Biomass Conv. Bioref.* 2 (2012) 285–296.
- [7] J. Kopyscinski, T.J. Schildhauer, S.M.A. Biollaz, *Production of synthetic natural gas (SNG) from coal and dry biomass – a technology review from 1950 to 2009*, *Fuel* 89 (2010) 1763–1783.
- [8] J.N. Dew, R.R. White, C.M. Slepcevic, *Hydrogenation of carbon dioxide on nickel-Kieselguhr catalyst*, *Ind. Eng. Chem.* 47 (1955) 140–146.
- [9] G.G. Binder, R.R. White, *Synthesis of methane from carbon dioxide and hydrogen*, *Chem. Eng. Progress* 46 (1950) 563–574.
- [10] J. Klose, M. Baerns, *Kinetics of the methanation of carbon monoxide on an alumina-supported nickel catalyst*, *J. Catal.* 85 (1984) 105–116.
- [11] J. Xu, G.F. Froment, *Methane steam reforming, methanation and water-gas shift: I. Intrinsic kinetics*, *Aiche J.* 35 (1989) 88–96.
- [12] G.D. Weatherbee, C.H. Bartholomew, *Hydrogenation of CO₂ on group VIII metals: II. Kinetics and mechanism of CO₂ hydrogenation on nickel*, *J. Catal.* 77 (1982) 460–472.
- [13] K. Jalama, *Carbon dioxide hydrogenation over nickel-, ruthenium-, and copper-based catalysts: review of kinetics and mechanism*, *Catal. Rev.* 59 (2017) 95–164.
- [14] S. Rönsch, J. Schneider, S. Matthischke, M. Schlüter, M. Götz, J. Lefebvre, P. Prabhakaran, S. Bajohr, *Review on methanation – from fundamentals to current projects*, *Fuel* 166 (2016) 276–296.
- [15] T. Kai, S. Furusaki, K. Yamamoto, *Kinetics of the methanation of carbon dioxide over a supported Ni-La₂O₃ catalyst*, *Can. J. Chem. Eng.* 66 (1988) 343–347.
- [16] H. Inoue, M. Funakoshi, *Kinetics of methanation of carbon monoxide and carbon dioxide*, *J. Chem. Eng. Jpn.* 17 (1984) 602–610.
- [17] R.A. Hubble, J.Y. Lim, J.S. Dennis, *Kinetic studies of CO₂ methanation over a Ni/γ-Al₂O₃ catalyst*, *Faraday Discuss.* 192 (2016) 529–544.
- [18] F. Koschany, D. Schlereth, O. Hinrichsen, *On the kinetics of the methanation of carbon dioxide on coprecipitated NiAl(O)_x*, *Appl. Catal. B* 181 (2016) 504–516.
- [19] J. Kopyscinski, T.J. Schildhauer, F. Vogel, S.M.A. Biollaz, A. Wokaun, *Applying spatially resolved concentration and temperature measurements in a catalytic plate reactor for the kinetic study of CO methanation*, *J. Catal.* 271 (2010) 262–279.
- [20] J. Zhang, N. Fatah, S. Capela, Y. Kara, O. Guerrini, A.Y. Khodakov, *Kinetic investigation of carbon monoxide hydrogenation under realistic conditions of methanation of biomass derived syngas*, *Fuel* 111 (2013) 845–854.
- [21] B. Mutz, M. Belimov, W. Wang, P. Sprenger, M.-A. Serrer, D. Wang, P. Pfeifer, W. Kleist, J.-D. Grunwaldt, *Potential of an alumina-supported Ni₃Fe catalyst in the methanation of CO₂ impact of alloy formation on activity and stability*, *ACS Catal.* 7 (2017) 6802–6814.
- [22] M.-A. Serrer, K.F. Kalz, E. Saraçi, H. Lichtenberg, J.-D. Grunwaldt, *Role of iron on the structure and stability of Ni_{3.2}Fe/Al₂O₃ during dynamic CO₂ methanation for P2X applications*, *ChemCatChem* 11 (2019) 5018–5021.
- [23] M. Belimov, D. Metzger, P. Pfeifer, *On the temperature control in a microstructured packed bed reactor for methanation of CO/CO₂ mixtures*, *AIChE J.* 63 (2017) 120–129.
- [24] H. Bakhtiary-Davijany, F. Hayer, X.K. Phan, R. Myrstad, H.J. Venvik, P. Pfeifer, A. Holmen, *Characteristics of an Integrated Micro Packed Bed Reactor-Heat Exchanger for methanol synthesis from syngas*, *Chem. Eng. J.* 167 (2011) 496–503.
- [25] F. Hayer, H. Bakhtiary-Davijany, R. Myrstad, A. Holmen, P. Pfeifer, H.J. Venvik, *Synthesis of dimethyl ether from syngas in a microchannel reactor—simulation and experimental study*, *Chem. Eng. J.* 167 (2011) 610–615.
- [26] R. Myrstad, S. Eri, P. Pfeifer, E. Rytter, A. Holmen, *Fischer-Tropsch synthesis in a microstructured reactor*, *Catal. Today* 147 (2009) S301–S304.
- [27] R. Berger, *EUROKIN spreadsheet on requirements for measurement of intrinsic kinetics in the gas-solid fixed-bed reactor* (2011).
- [28] O.A. Hougen, K.M. Watson, *Solid catalysts and reaction rates*, *Ind. Eng. Chem* 43 (1943) 529–541.
- [29] S. Tauro, *One-step Synthesis of Dimethyl Ether Using Microreactors*, Shaker Verlag GmbH, 2014.
- [30] J. Nocedal, S.J. Wright, *Numerical optimization*, Springer, New York, NY, 2000.
- [31] D.C. Montgomery, *Design and analysis of experiments*, 8th ed., John Wiley & Sons Inc, Hoboken NJ, 2013.
- [32] G. Schwarz, *Estimating the dimension of a model*, *Ann. Stat.* 6 (1978) 461–464.
- [33] H. Akaike, *A new look at the statistical model identification*, *IEEE Trans. Autom. Control* 19 (1974) 716–723.
- [34] C. Vogt, E. Groeneveld, G. Kamsma, M. Nachtgeaal, L. Lu, C.J. Kiely, P.H. Berben, F. Meirer, B.M. Weckhuysen, *Unravelling structure sensitivity in CO₂ hydrogenation over nickel*, *Nat. Catal.* 1 (2018) 127–134.
- [35] S.-I. Fujita, M. Nakamura, T. Doi, N. Takezawa, *Mechanisms of methanation of carbon dioxide and carbon monoxide over nickel/alumina catalysts*, *Appl. Catal. A* 104 (1993).
- [36] D.C. Gardner, C.H. Bartholomew, *Kinetics of carbon deposition during methanation of carbon monoxide*, *Ind. Eng. Chem* 20 (1981) 80–87.
- [37] J.G. McCarty, H. Wise, *Hydrogenation of surface carbon on alumina-supported nickel*, *J. Catal.* 54 (1979) 406–416.
- [38] R.E. Hayes, W.J. Thomas, K.E. Hayes, *A study of the nickel-catalyzed methanation reaction*, *J. Catal.* 92 (1985) 312–326.
- [39] Wheeler, C.A. Jhalani, E.J. Klein, S. Tummala, L.D. Schmidt, *The water-gas-shift reaction at short contact times*, *J. Catal.* 223 (2004) 191–199.
- [40] R.J. Byron Smith, M. Loganathan, M.S. Shantha, *A review of the water gas shift reaction kinetics*, *Int. J. Chem. Reactor Eng.* 8 (2010).
- [41] S.A. Theofanidis, V.V. Galvita, H. Poelman, G.B. Marin, *Enhanced carbon-resistant dry reforming Fe-Ni catalyst: role of Fe*, *ACS Catal.* 5 (2015) 3028–3039.
- [42] A. Winkler, K.D. Rendulic, *Adsorption kinetics for hydrogen adsorption on nickel and coadsorption of hydrogen and oxygen*, *Surf. Sci.* 18 (1982) 19–31.